Article

Speed Regulation for PMSM with Super-Twisting Sliding-Mode Controller via Disturbance Observer

Mingyuan Hu [1] **, Hyeongki Ahn** [2] **, Yoonuh Chung** [2] **and Kwanho You** [1,2,*]

1   Department of Smart Fab. Technology, Sungkyunkwan University, Suwon 16419, Republic of Korea; hmy160831@g.skku.edu
2   Department of Electrical and Computer Engineering, Sungkyunkwan University, Suwon 16419, Republic of Korea; ahk5721@skku.edu (H.A.); jordan53@g.skku.edu (Y.C.)
*   Correspondence: khyou@skku.edu; Tel.: +82-31-290-7148

Abstract: This paper focuses on the speed regulation of a permanent-magnet synchronous motor (PMSM) with an uncertain extended load disturbance. A novel super-twisting sliding-mode control (NSTSMC) was proposed via a nonlinear integral sliding surface and a modified reaching law, effectively suppressing the chattering phenomenon. In addition, the NSTSMC can improve the convergence performance with a 0.04 s settling time, satisfying the super-twisting algorithm stability condition. For the novel integral sliding surface, the integral power term of the system state variables was incorporated into the conventional sliding surface to effectively improve the convergence rate and anti-disturbance ability. Moreover, an extended sliding-mode disturbance observer (ESO) was used to estimate the lumped extended disturbance and add the corresponding feedback compensation value from the sliding-mode disturbance observer to the output of the speed controller for the improved robustness of the system. The ESO-NSTSMC was developed to improve the performance of PMSM speed regulation by combining the advantages of the novel integral sliding surface, achieving a settling time of 0.01 s without overshoot. We confirm the performance of the proposed NSTSMC through a PMSM speed simulation and demonstrate that the controller can enhance the dynamic performance and robustness of the system.

Keywords: PMSM; integral sliding surface; super-twisting algorithm; disturbance observer

MSC: 93C10; 93C40; 93C73

1. Introduction

Permanent-magnet synchronous motors (PMSMs) have received widespread attention among the various types of AC synchronous motors due to their advantages of low acoustic noise, high power density, lofty torque-current ratio, and simple structure [1–3]. Due to its advantageous characteristics and wide applications in industry, a PMSM as the control object has become a research hotspot, as introduced in [4,5]. However, the existence of parameter perturbations, system uncertainties, and unavoidable external disturbances in the speed regulation system of the PMSM makes it difficult to simultaneously obtain excellent anti-disturbance properties and achieve high-precision speed-tracking performance using the conventional linear control methods such as the linear proportional-integral control algorithm and linear quadratic-regulator control [6,7]. With the rapid development of modern control theories, various nonlinear advanced control strategies and algorithms have been applied to the PMSM system, including robust control [8], active disturbance rejection control [9,10], H_∞ control [11], and sliding-mode control (SMC) [12,13].

Due to its insensitivity to uncertainties and disturbances, SMC is considered one of the most effective strategies for dealing with uncertain nonlinear systems among the existing advanced control algorithms, and fast dynamic responses and strong robustness can also be achieved with SMC [14–16]. Since conventional SMC cannot converge to the equilibrium

point in finite time, terminal SMC was developed [17], where the tracking error can be steered to the equilibrium point in finite time. Furthermore, nonsingular terminal SMC was designed to solve the singularity problem of terminal SMC for the PMSM system [18]. In [19], a new control strategy called the dual-time-scale SMC method for PMSM was proposed. Based on the quasi-steady-state theory, two parallel SMCs were used to control the PMSM rather than the conventional velocity-current dual-loop control.

However, the most prominent drawback of conventional SMC in previous studies was the steady-state inaccuracies and chattering phenomena caused by discontinuous control actions [20]. To reduce this tendency, many control strategies have been proposed [21–23]. With the development of SMC theory and the requirement for high-precision control, an effective way to reduce chattering is to use high-order SMC techniques [24]. Since the integrator in the super-twisting algorithm (STA) can smoothen discontinuous signals, super-twisting SMC ensures higher accuracy in tracking performance and the simultaneous damping of chattering phenomena for PMSM for which the STA is best known [25].

However, the SMC algorithm must choose a large control gain to provide adequate control strength and restrain the adverse effects of disturbances [26], which can result in the suboptimal dynamic and steady-state performance of the PMSM system. In addition, the upper limit of the disturbances presented in the control systems of the PMSM cannot be directly measured or estimated in practical applications [27], which worsens the chattering phenomenon when the gain of the sliding-mode controller becomes much larger [28].

To solve these problems, an effective approach to overcome this difficulty is to use composite control techniques [29,30]. Since disturbance observers can handle external disturbances, they can be used to improve the control performance of the system [31]. By using a disturbance observer (DOB) to estimate the unknown incidental disturbances and compensate for the estimates of SMC, better control performance can be achieved without the need for a large control gain [32]. Due to the advantages of the ESO in terms of its ease of application and robustness, many studies have shown that the expected estimation performance is achieved using the interference observer with the sliding-mode technique [33,34].

Based on the above research, in this study, a composite NSTSMC scheme is designed by introducing a DOB and combining it with an NSTSMC algorithm to obtain better performance for the speed-regulation problem of a PMSM system. We design a new finite-time integral sliding surface and calculate its finite time. Moreover, a new reaching law is added to the NSTSMC to improve the chattering phenomenon. The main contributions of this work can be summarized as follows:

- Since the proposed nonlinear sliding surface makes the state of the control object reach the equilibrium point quickly, we propose a novel nonlinear sliding surface by developing a terminal attractor for SMC.
- The proposed NSTSMC incorporates the STA to reduce chattering and improve the control performance of the PMSM.
- The finite time is calculated via the novel sliding surface.
- The ESO is incorporated into the NSTSMC to suppress overshoot and oscillation for the control precision of the PMSM.

The rest of this study is organized as follows. In Section 2, the mathematical model for the three-phase PMSM and external disturbances is introduced. To estimate the unknown lumped disturbance and compensate for the estimated value of SMC, the ESO is introduced in Section 3. In Section 4, the proposed novel integral sliding surface based on a terminal term is shown, and the adaptive super-twisting algorithm and analysis of system stability using the strong Lyapunov function are discussed. In Section 5, the effectiveness of the proposed methods is verified using simulations. Finally, the conclusions are presented in Section 6.

2. Mathematical Model of PMSM

The mathematical model of the surface-mounted PMSM (SPMSM) in the reference coordination is represented as follows [20]:

$$
\begin{aligned}
V_d &= Ri_d + L_s \frac{di_d}{dt} - p_n\omega_m L_s i_q, \\
V_q &= Ri_q + L_s \frac{di_q}{dt} + p_n\omega_m L_s i_d + p_n\omega_m\psi_f, \\
J\frac{d\omega_m}{dt} &= \frac{3p_n\psi_f}{2}i_q - T_L - B\omega_m,
\end{aligned}
\tag{1}
$$

whose parameters are listed in Table 1.

Table 1. Parameters of the dynamical model of the PMSM.

System Parameters	Unit	Description
V_d, V_q	V	d-axis and q-axis stator voltages
i_d, i_q	A	d-axis and q-axis stator currents
ω_m	rad/sec	electrical rotor angular velocity
R_s	Ω	stator resistance
L_s	H	stator inductance
J	kg $\cdot$ m^2	rotor-equivalent inertia
B	N $\cdot$ m $\cdot$ s/rad	viscous friction coefficient
ψ_f	Wb	magnetic flux
p_n		number of poles
T_L	N $\cdot$ m	load torque

For SPMSM, good control performance can be achieved using the rotor magnetic field orientation control (FOC) method with $i_d = 0$. Therefore, Equation (1) can be rewritten into the mathematical model as

$$
\begin{aligned}
\frac{di_q}{dt} &= \frac{1}{L_s}(-Ri_q - p_n\psi_f\omega_m + V_q), \\
\frac{d\omega_m}{dt} &= \frac{1}{J}\left(-B\omega_m - T_L + \frac{3p_n\psi_f}{2}i_q\right).
\end{aligned}
\tag{2}
$$

To change the dynamical model of rotational speed in Equation (2) into a state-space form, the state variable regarding ω_{cmd} and ω_m must be defined as follows:

$$
\begin{aligned}
x_1 &= \omega_{cmd} - \omega_m, \\
x_2 &= \dot{x}_1 = \dot{\omega}_{cmd} - \dot{\omega}_m,
\end{aligned}
\tag{3}
$$

where ω_{cmd} and ω_m are the reference and actual angular velocities, respectively. In general, $\dot{\omega}_{cmd} = \ddot{\omega}_{cmd} = 0$ as ω_{cmd} is designed to be a constant. By combining Equations (2) and (3), $\dot{x}_1$ and $\dot{x}_2$ can be redefined as follows:

$$
\begin{aligned}
\dot{x}_1 &= \dot{\omega}_{cmd} - \dot{\omega}_m = \dot{\omega}_{cmd} + \frac{1}{J}\left(B\omega_m + T_L - \frac{3p_n\psi_f}{2}i_q\right), \\
\dot{x}_2 &= \ddot{\omega}_{cmd} - \ddot{\omega}_m = \ddot{\omega}_{cmd} - \frac{3p_n\psi_f}{2J}\cdot\frac{di_q}{dt} + \frac{B}{J}\dot{\omega}_m + \frac{\dot{T}_L}{J}.
\end{aligned}
\tag{4}
$$

Here, $u = di_q/dt$, $a = B/J$, and $b = 3p_n\psi_f/2J$ are defined, and Equation (4) is transferred to a state-space form, as in Equation (5).

$$
\begin{aligned}
\dot{x}_1 &= x_2, \\
\dot{x}_2 &= -ax_2 - bu + d(t),
\end{aligned}
\tag{5}
$$

where $d(t) = \dot{T}_L/J + \ddot{\omega}_{cmd} + (B/J)\dot{\omega}_{cmd}$ is the lumped extended disturbance. During the actual application of a PMSM, it is difficult to effectively measure the load disturbance value. Therefore, we assume that the lumped extended disturbance is globally bounded and define it as $\bar{d} = \sup|d(t)|$ for $t > 0$.

3. Design of Extended Sliding-Mode Disturbance Observer

The extended sliding-mode disturbance observer technique is presented for the PMSM control system [35]. By using the ESO, external load disturbances are subsequently applied as feedback to the NSTSMC after being estimated online. Figure 1 shows the structure of the ESO and the detailed procedure is demonstrated in the following description. Compared to the system state that changes in each sampling cycle of the speed loop, the system perturbations are regarded as considerably slow in a real PMSM-driven system. Therefore, the derivative of $d(t)$ in Equation (2) can be considered $\dot{d}(t) = 0$ with respect to time (t). The state-space equations of the system can be expressed as in Equation (6), with the mechanical rotor angular velocity (ω_m) and external disturbances ($d(t)$) as state variables, the electromagnetic torque (T_e) as the control input, and the external disturbance as the system output.

$$
\begin{bmatrix} \dot{\omega}_m \\ \dot{d} \end{bmatrix} = \begin{bmatrix} -\frac{B}{J} & -\frac{1}{J} \\ 0 & 0 \end{bmatrix} \begin{bmatrix} \omega_m \\ d \end{bmatrix} + \begin{bmatrix} \frac{1}{J} \\ 0 \end{bmatrix} T_e,
$$
$$
y = \begin{bmatrix} 0 & 1 \end{bmatrix} \begin{bmatrix} \omega_m \\ d \end{bmatrix}.
$$
(6)

The ESO equation can be expressed as in Equation (7), where the mechanical rotor angular velocity (ω_m) and the external load disturbance $d(t)$ are taken as estimates.

$$
\begin{bmatrix} \dot{\hat{\omega}}_m \\ \dot{\hat{d}} \end{bmatrix} = \begin{bmatrix} -\frac{B}{J} & -\frac{1}{J} \\ 0 & 0 \end{bmatrix} \begin{bmatrix} \hat{\omega}_m \\ \hat{d} \end{bmatrix} + \begin{bmatrix} -\frac{1}{J} \\ 0 \end{bmatrix} T_e + \begin{bmatrix} 1 \\ l \end{bmatrix} \eta(e_{do}),
$$
(7)

where l is the observer gain. By taking the speed observation error as $e_{do} = \omega_m - \hat{\omega}_m$, $\eta(e_{do})$ is treated as the sliding-mode function. The equation of the observation error via Equations (6) and (7) is given by

$$
\dot{e}_{do} = -\frac{B}{J} e_{do} - \frac{1}{J} e_{dis} - \eta(e_{do}),
$$
$$
\dot{e}_{dis} = -l \cdot \eta(e_{do}),
$$
(8)

where $e_{dis} = d - \hat{d}$ is the observation error for the external load disturbance. The sliding surface is demonstrated for this ESO as follows:

$$
\sigma_\omega(t) = e_{do}(t) + \lambda_1 \int_0^t e_{do}(\tau)d\tau
$$
(9)

where λ_1 is a positive scalar. The exponential reaching law based on the boundary layer method is adopted to reduce the chattering from using the ESO.

$$
\dot{\sigma}_\omega = -k_\omega \text{sat}(\sigma_\omega) - k_{t\omega}\sigma_\omega,
$$
(10)

where $k_{t\omega} > 0$ is the exponential coefficient of the convergence law and $k_\omega > 0$ is the switching gain. By using $-e_{dis}/J$ as the perturbation term and substituting Equation (10) into Equation (11), the sliding-mode function $\eta(e_{do})$ can be written as

$$
\eta(e_{do}) = \left(\lambda_1 - \frac{B}{J} \right) \cdot e_{do} + k_\omega \text{sat}(\sigma_\omega) + k_{t\omega}\sigma_\omega.
$$
(11)

The following conditions are satisfied when the observer trajectory reaches and stays on the sliding surface $\sigma_\omega = 0$ within a finite time.

$$\begin{aligned} \sigma_\omega &= \dot{\sigma}_\omega = 0, \\ e_{do} &= \dot{e}_{do} = 0. \end{aligned} \tag{12}$$

Combining Equations (8) and (12) yields the equation of the observation error, and Equation (13) is as follows:

$$\begin{aligned} e_{dis} &= -J \cdot \eta(e_{do}), \\ \dot{e}_{dis} &= -l \cdot \eta(e_{do}). \end{aligned} \tag{13}$$

Therefore, based on Equation (13), the estimation error of the external load disturbance with respect to time is given by

$$e_{dis} = c_d e^{\frac{l}{J}t}, \tag{14}$$

where c_d is a positive constant. The observer gain should satisfy $l < 0$ to guarantee that the observation error of the external load disturbance converges to zero. In addition, the observer gain is related to the convergence speed of the estimation error. The Lyapunov function is defined below to ensure the stability of the ESO.

$$V_1 = \frac{1}{2}\sigma_\omega^2. \tag{15}$$

By differentiating V_1 with respect to time (t) and applying the control law in Equation (11), the following equation can be obtained:

$$\begin{aligned} \dot{V}_1 &= \sigma_\omega \cdot \dot{\sigma}_\omega \\ &= \sigma_\omega\left(-\frac{B}{J}e_{do} - \frac{1}{J}e_{dis} - \eta(e_{do}) + \lambda e_\omega\right) \\ &= \sigma_\omega\left(-\frac{1}{J}e_{dis} - k_\omega\mathrm{sat}(\sigma_\omega)\right) - k_{t\omega}\sigma_\omega^2. \end{aligned} \tag{16}$$

To satisfy the finite-time Lyapunov stability theorem $\dot{V} < 0$ for Equation (16), the condition of the control gain is chosen as

$$k_\omega + k_{t\omega}\varepsilon_\omega > \frac{1}{J}|e_{dis}|, \tag{17}$$

where ε_ω is the layer thickness of Equation (10). Based on Equation (17), the ESO is asymptotically stable at an appropriate observer gain while the observer trajectory moves and approaches the sliding-mode surface within a finite time. Figure 2 shows how the ESO is embedded in the NSTSMC. Figure 3 illustrates the schematic structure of the entire PMSM system.
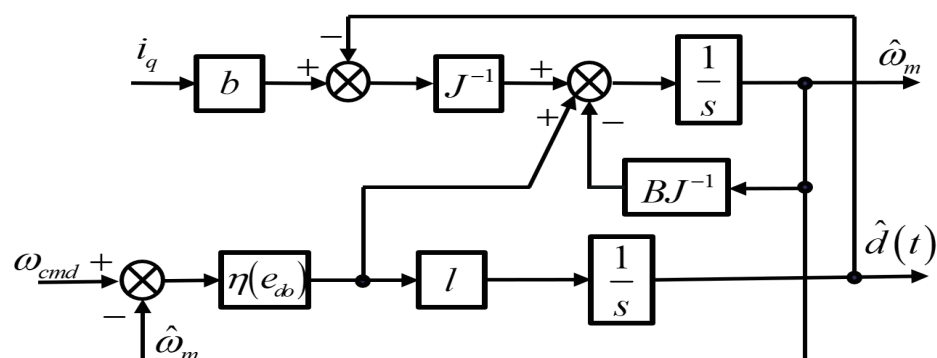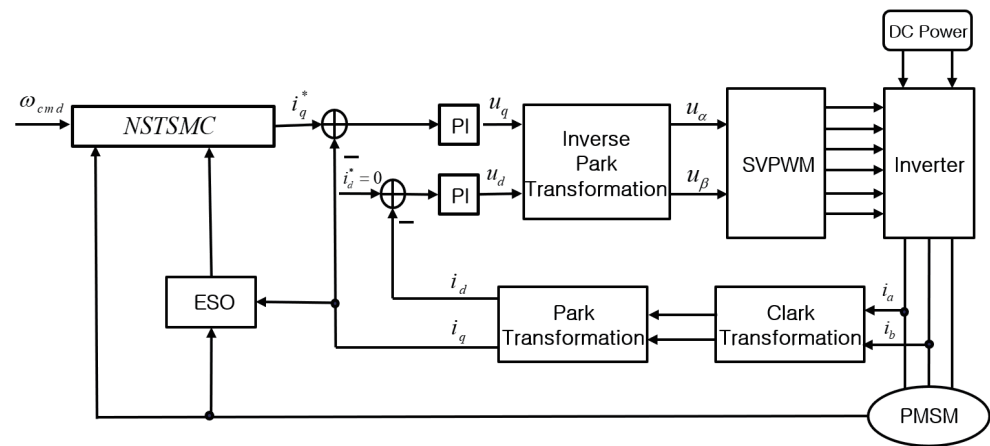

Figure 1. Block diagram of ESO.
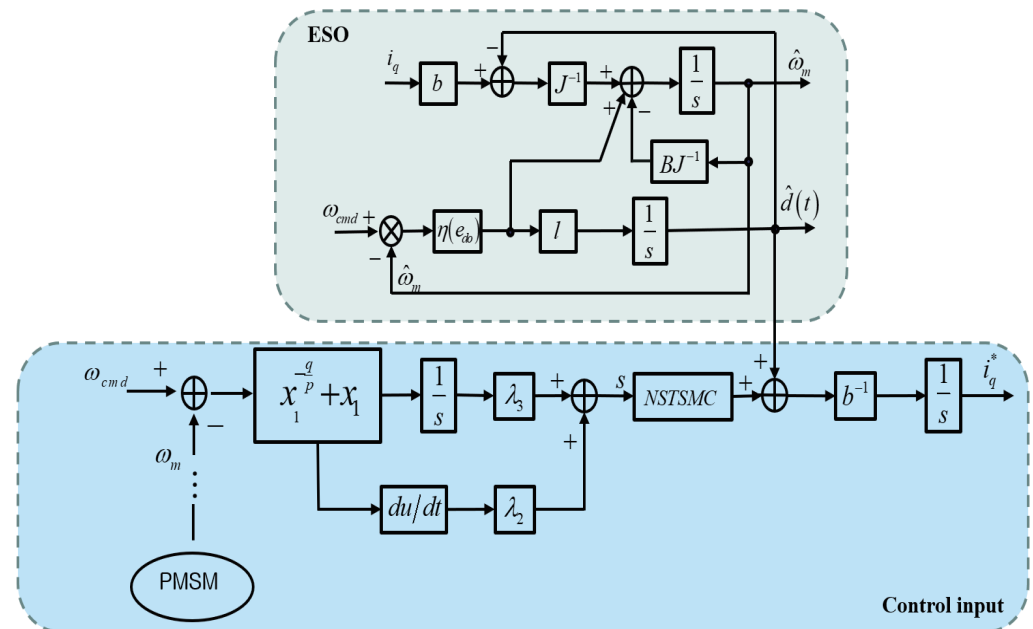
Figure 2. ESO-embedded NSTSMC structure diagram.

Figure 3. Block diagram of PMSM system based on the NSTSMC with the ESO scheme.

4. Design of PMSM Speed Controller

4.1. Design of a Novel Integral Sliding Surface

To improve the convergence speed and robustness, a novel integral sliding surface (NSS) is proposed as follows:

$$\sigma = \lambda_2 x_2 + \lambda_3 \int_0^t (x_1^{-\frac{q}{p}} + \lambda_4 x_1) d\tau, \tag{18}$$

where $\lambda_2 > 0$, $\lambda_3 > 0$, $\lambda_4 < 0$, and $q > p > 0$. Equation (18) becomes zero when the initial state arrives at the sliding surface (σ). Equation (18) can be obtained after rearranging Equation (19) when $\sigma = 0$, as follows:

$$\dot{x}_1 = \frac{\lambda_3}{\lambda_2} \left[\frac{p}{p-q} x_1(0)^{1-\frac{q}{p}} + \frac{\lambda_4}{2} x_1^2(0) \right]. \tag{19}$$

We can obtain t_s by taking an integral from 0 to the convergence time (t_s) and from $x(0)$ to $x(t_s)$ for Equation (19), as follows:

$$t_s = \frac{2\lambda_2(q-p)}{2p\lambda_3|x_1(0)|^{-\frac{q}{p}} + \lambda_3\lambda_4(p-q)|x_1(0)|}. \tag{20}$$

4.2. Design of Novel Reaching Law

To address the chattering phenomenon, the super-twisting algorithm (STA) with a perturbation term is introduced, which can be written as follows [36]:

$$\begin{aligned} \dot{\sigma} &= -k_1|\sigma|^{\frac{1}{2}}\mathrm{sgn}(\sigma) - k_2\sigma + z, \\ \dot{z} &= -k_3\mathrm{sgn}(\sigma) + \dot{\vartheta}, \end{aligned} \tag{21}$$

where k_1, k_2, and k_3 represent the positive scalar. Moreover, σ stands for the sliding surface calculated using Equation (18). The perturbation term $\vartheta = \lambda_2\left[d(t) - \hat{d}(t)\right]$ is supposed to be bounded as $|\dot{\vartheta}| \leq \rho$ with $\rho > 0$. Based on the STA, a novel super-twisting algorithm called the NSTA is proposed as follows:

$$\begin{aligned} \dot{\sigma} &= -k_1|\sigma|^{\frac{1}{2}}\mathrm{sgn}(\sigma) - k_2\eta_1(t)\sigma + z \\ \dot{z} &= -k_3\eta_2(t)\mathrm{sgn}(\sigma) + \dot{\vartheta}, \end{aligned} \tag{22}$$

where, $\eta_1(t)$ and $\eta_2(t)$ represent the adaptive terms, as in Equations (23) and (24), and $0 < \varepsilon < 1$, $k_0 > 0$. $\eta_1(t)$ and $\eta_2(t)$ are globally bound and defined as $\bar{\eta}_1 = \sup \eta_1(t)$ and $\bar{\eta}_2 = \sup \eta_2(t)$, respectively, for $t > 0$.

$$\eta_1(t) = \frac{1}{\varepsilon + \left(k_0 + \frac{1}{|\sigma|} - \varepsilon\right)e^{-|\sigma|}}. \tag{23}$$

The property of $\eta_1(t)$, which was introduced in [37], is that $\eta_1(t)$ converges to a value of $1/\varepsilon$ greater than 1 if $|\sigma|$ increases. Therefore, $\eta_1(t)$ indicates that faster arrival times can be obtained after joining Equation (22). On the contrary, the denominator term of $\eta_1(t)$ converges to $k_o + 1/|\sigma|$ if $|\sigma|$ decreases and $\eta_1(t)$ converges to $|\sigma|/(k_o|\sigma|+1)$, where the system state $|\sigma|$ decreases to zero under the control inputs proposed in the subsequent section. This indicates that $\eta_1(t)$ decreases to zero to suppress chattering when the system trajectory approaches the sliding surface. By varying $\eta_1(t)$ between $1/\varepsilon$ and zero, the controller designed based on the proposed convergence law can dynamically adapt to changes in the sliding surface and the system state $|\sigma|$.

$$\eta_2(t) = \frac{1}{\varepsilon + (\varepsilon - 1)e^{-|\sigma|}}. \tag{24}$$

Based on [38], ε is a strictly positive offset that is less than 1. The parameter function given by Equation (24) does not affect the stability of the control since $\eta_2(t)$ is always strictly positive. If $|\sigma|$ increases, $\eta_2(t)$ approaches $1/\varepsilon$; therefore, $1/\eta_2(t)$ converges to ε, which is less than 1 via Equation (24). This means that the convergence speed of the sliding surface will be faster as $\eta_2(t)$ increases during the reaching mode. Meanwhile, $\eta_2(t)$ approaches 1 if $|\sigma|$ decreases; thus, $\eta_2(t)$ converges to 1. This means that $1/\eta_2(t)$ is gradually reduced to limit the chattering as the system approaches the sliding surfaces. Consequently, the ERL allows the controller to vary between 1 and $1/\varepsilon$ by allowing $1/\eta_2(t)$ to dynamically adapt to changes in the switching function. By combining the advantages of Equations (23) and (24), if $|\sigma|$ increases, $k_2\eta_1$ and $k_3\eta_2$ converge to k_2/ε and $k_3\varepsilon$ in the NSTSMC, respectively. Meanwhile, if $|\sigma|$ decreases, $k_2\eta_1$ and $k_3\eta_2$ converge to k_2 and 0, respectively. By selecting a small gain of k_2, the system control performance can be satisfied,

and the divergent influence is removed by the integral term $k_3\eta_2\text{sgn}(\sigma)$. By combining Equations (5), (18) and (22), the NSTSMC without a perturbation term is given by

$$
\begin{aligned}
i_q = \frac{1}{b}\int_0^t \Bigg(&-ax_2 + \frac{\lambda_3}{\lambda_2}(x_1^{-\frac{q}{p}} + \lambda_4 x_1) + \alpha|\sigma|^{\frac{1}{2}}\text{sgn}(\sigma) \\
&+\beta\eta_1(t)\sigma + \int_0^t \gamma\eta_2(t)\text{sgn}(\sigma)d\tau_1 \Bigg)d\tau_2.
\end{aligned}
\tag{25}
$$

Since the performance of the anti-disturbance characteristics of the controller can be improved by combining the estimated values, the performance of the anti-disturbance characteristics of the controller can be improved by combining the estimated values of the ESO and Equation (25). Therefore, the proposed NSTSMC is given by

$$
\begin{aligned}
i_q^* = \frac{1}{b}\int_0^t \Bigg(&-ax_2 + \frac{\lambda_3}{\lambda_2}(x_1^{-\frac{q}{p}} + \lambda_4 x_1) + \alpha|\sigma|^{\frac{1}{2}}\text{sgn}(\sigma) \\
&+\beta\eta_1(t)\sigma + \int_0^t \gamma\eta_2(t)\text{sgn}(\sigma)d\tau_1 + \hat{d}(t) \Bigg)d\tau_2.
\end{aligned}
\tag{26}
$$

4.3. Stability Analysis of Controller

The candidate Lyapunov function for the speed controller is given by

$$
V_2 = \xi^T P \xi,
\tag{27}
$$

where the vector ξ^T is $[\xi_1\ \xi_2] = [|\sigma|^{\frac{1}{2}}\text{sgn}(\sigma)\ z]$. The NSTA with the disturbance is obtained as

$$
\begin{aligned}
\dot{\sigma} &= -[k_1 + \delta_1(t)]|\sigma|^{\frac{1}{2}}\text{sgn}(\sigma) + z, \\
\dot{z} &= -\delta_2(t)\text{sgn}(\sigma) + \dot{\vartheta}.
\end{aligned}
\tag{28}
$$

Here, $\delta_1(t) = k_2\eta_1(t)|\sigma|^{\frac{1}{2}}$, $\delta_2(t) = k_3\eta_2(t)$ are globally bound by $\bar{\delta}_1 = \sup\delta_1(t)$ and $\bar{\delta}_2 = \sup\delta_2(t)$ with $t > 0$, respectively. By taking the derivative of the vector ξ^T, Equation (29) is given by

$$
\dot{\xi} = \frac{1}{|\xi_1|}A\xi + \frac{1}{|\xi_1|}E(|\xi_1|\dot{\vartheta}),
\tag{29}
$$

where matrices A and E are

$$
A = \begin{bmatrix} \frac{k_1+\delta_1(t)}{2} & \frac{1}{2} \\ -\delta_2(t) & 0 \end{bmatrix}, \quad E = \begin{bmatrix} 0 \\ 1 \end{bmatrix}.
\tag{30}
$$

Matrix P can be obtained via the strong Lyapunov function, which is expressed as

$$
P = \begin{bmatrix} 2\delta_2(t) + \frac{(k_1+\delta_1(t))^2}{2} & -\frac{k_1+\delta_1(t)}{2} \\ -\frac{k_1+\delta_1(t)^2}{2} & 1 \end{bmatrix}.
\tag{31}
$$

Equation (32) is obtained by taking the derivative of Equation (27) as follows:

$$
\begin{aligned}
\dot{V}_2 &= \dot{\xi}^T P \xi + \xi^T P \dot{\xi}, \\
&= \frac{1}{|\xi_1|}\left[\xi^T A^T P \xi + \xi^T P A \xi + (|\xi_1|\dot{\vartheta})E^T P \xi + (|\xi_1|\dot{\vartheta})\xi^T P E\right].
\end{aligned}
\tag{32}
$$

Equation (32) can be rewritten in an inequality form in terms of the assumption on the bounded perturbation as follows:

$$
\dot{V}_2 \leq \frac{1}{|\xi_1|}\left(\xi^T A^T P \xi + \xi^T P A \xi + \rho^2|\xi_1|^2 + \xi^T P E E^T P \xi\right).
\tag{33}
$$

$\rho^2|\xi_1|^2$ can be switched to $\rho^2\xi^T C^T C\xi$ after defining $C = \begin{bmatrix} 1 & 0 \end{bmatrix}$. By substituting $\rho^2|\xi_1|^2$ into Equation (33), Equation (34) is derived as

$$\dot{V}_2 \le \frac{1}{|\xi_1|}\left(\xi^T A^T P\xi + \xi^T PA\xi + \rho^2\xi^T C^T C\xi + \xi^T PEE^T P\xi\right). \tag{34}$$

Using the algebraic Lyapunov equation, Equation (34) can be rewritten as

$$\dot{V}_2 \le -\frac{1}{|\xi_1|}\xi^T Q\xi, \tag{35}$$

where $Q = -\left(A^T P + PA + \rho^2 C^T C + PEE^T P\right)$. $k_1 + \delta_1^*$ is defined by λ, where λ is an arbitrary positive scalar. Matrices A and P can be rewritten in the following form:

$$A = \begin{bmatrix} \frac{\lambda}{2} & \frac{1}{2} \\ -\delta_2^* & 0 \end{bmatrix}, \quad P = \begin{bmatrix} 2\delta_2^* + \frac{\lambda^2}{2} & -\frac{\lambda}{2} \\ -\frac{\lambda}{2} & 1 \end{bmatrix}. \tag{36}$$

Matrix Q presented in Equation (37) can be calculated using matrices A, E, C, and P as

$$Q = \begin{bmatrix} -\frac{\lambda^3}{2} - \frac{\lambda^2}{4} + 3\delta_2^*\lambda - \rho^2 & \frac{\lambda}{2} \\ \frac{\lambda}{2} & \frac{\lambda}{2} - 1 \end{bmatrix}. \tag{37}$$

If $Q > 0$, $\dot{V} < 0$. Using leading principal minors, the conditions to be stable are given by

$$\begin{aligned} &k_1 > 2 - \delta_1^*, \\ &k_3 > \frac{\lambda^4}{2\eta_2^*(3\lambda^2 - 6\lambda)} - \frac{\lambda^3}{4\eta_2^*(\lambda^2 - 2\lambda)} + \frac{\lambda\rho^2}{\eta_2^*(3\lambda^2 - 6\lambda)} - \frac{2\rho^2}{\eta_2^*(3\lambda^2 - 6\lambda)}, \\ &\lambda > 2. \end{aligned} \tag{38}$$

4.4. Overall Stability Analysis including the Disturbance Observer and Controller

As the disturbance observer and controller are included in this study, the stability of the entire speed loop must be guaranteed, including the ESO and NSTSMC. The candidate Lyapunov function (V_{all}) for the overall system using Equations (15) and (27) is expressed as

$$V_{all} = \sum_{i=1}^{n} V_i, n = 1, 2. \tag{39}$$

By taking the derivative of Equation (39), Equation (40) is given as follows:

$$\dot{V}_{all} = \sum_{i=1}^{n} \dot{V}_i, n = 1, 2. \tag{40}$$
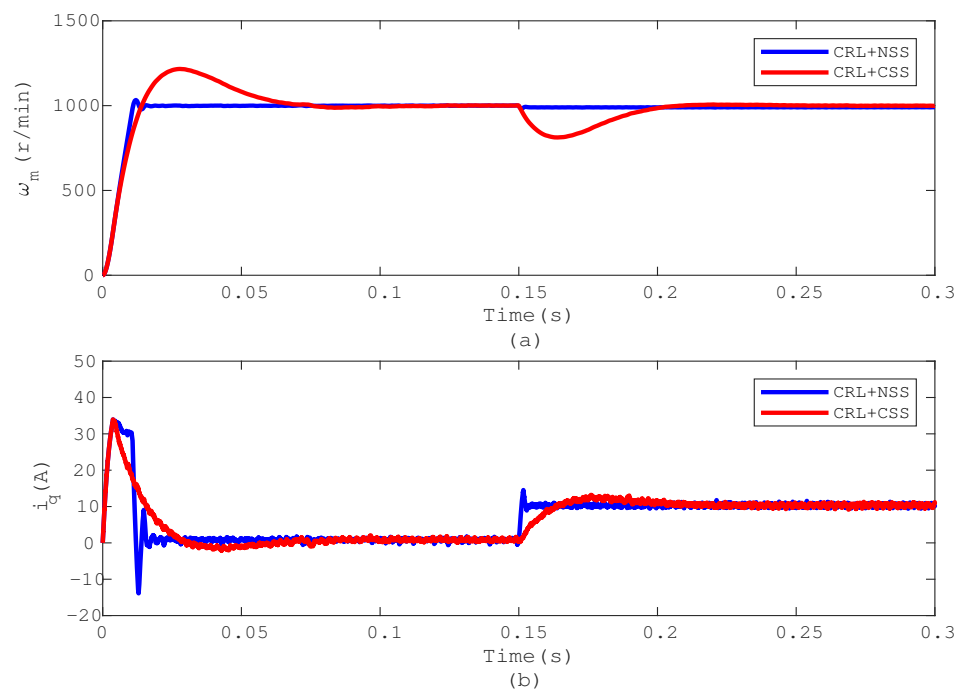
By using Equations (16) and (35), $\dot{V}_{all} < 0$ is satisfied. Therefore, the stability of the entire speed loop can be guaranteed.

5. Simulation

Table 2 summarizes the parameter values of the PMSM. We carried out performance comparison tests to effectively present our proposed ESO-NSMC. In case I, we compared the performance of conventional reaching law (CRL) + conventional sliding surface (CSS) and CRL+NSS, as shown in Figure 4. In Figure 4a, the simulation time was set to 0.3 s and the motor starting load torque was set to 0 N·m. The load torque suddenly increased to 10 N·m at 0.15 s. The simulation results illustrate that CRL+NSS approaches the target speed faster than CRL + CSS for the same control gain, as shown in Figure 4a. The corresponding current change, which represents the change in the control action, is shown in Figure 4b.

Table 2. Parameter values of the PMSM.

Parameter	Value	Unit
Resistance R_s	2.875	$[\Omega]$
Inductance L_s	8.5	[mH]
Magnetic flux ψ_f	0.175	[Wb]
Inertia J	0.0003	$[\text{kg} \cdot \text{m}^2]$
Viscous friction coefficient B	0.0008	$[\text{N} \cdot \text{m} \cdot \text{s} / \text{rad}]$
Pole pairs n_p	4	
Reference speed ω_{cmd}	1000	[r/min]
Sampling time T_s	1×10^{-5}	[s]

Figure 4. Comparison of CRL+NSS and CRL+CSS: (**a**) speed regulation, (**b**) control action.

In case II, the conventional super-twisting algorithm (CSTA) with NSS was compared to the CRL+NSS, as shown in Figure 5. The simulation times were set to the same as those shown in Figure 4, that is, 0.15 and 0.4 s, respectively. For speed regulation, the comparison of the CSTA+NSS without overshoot and the CRL+NSS is presented in Figure 5a. Figure 5b shows the current change with respect to the speed change. For case III, speed regulation and speed tracking, including the corresponding current (control action) changes, are illustrated in Figures 6 and 7, respectively. In Figure 6a, the performance of the NSTA with NSS and the CSTA with NSS for speed regulation is compared. The NSTA with NSS can track 1000 rpm in 0.01 s, which is faster than the CRL+NSS. Moreover, the current via the NSTA+NSS can change and approach the desired value more quickly compared to the CSTA+NSS, as shown in Figure 6b. Figure 7a shows the speed-tracking results using the same control strategy shown in Figure 6a. Figure 7a illustrates that the NSTA with NSS adapts better to speed changes when the desired speed drops from 800 rpm to 400 rpm in 0.05 s and increases from 400 rpm to 1200 rpm in 0.1 s. Compared to the CSTA+NSS, the current in the NSTA+NSS can change to the desired value quickly and smoothly, as shown in Figure 7b.
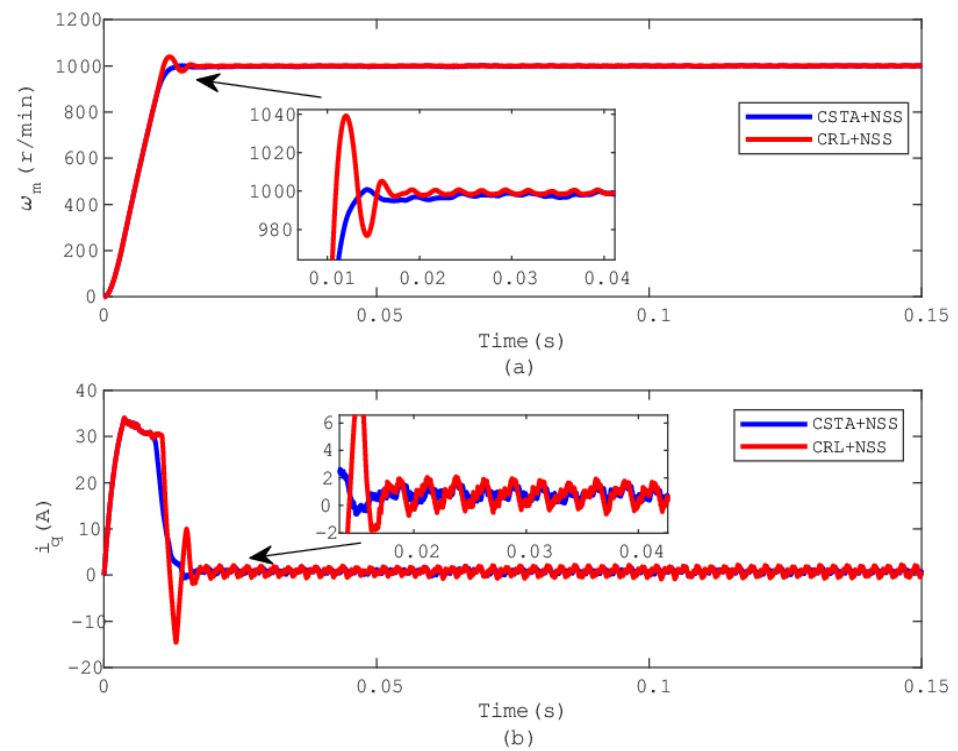
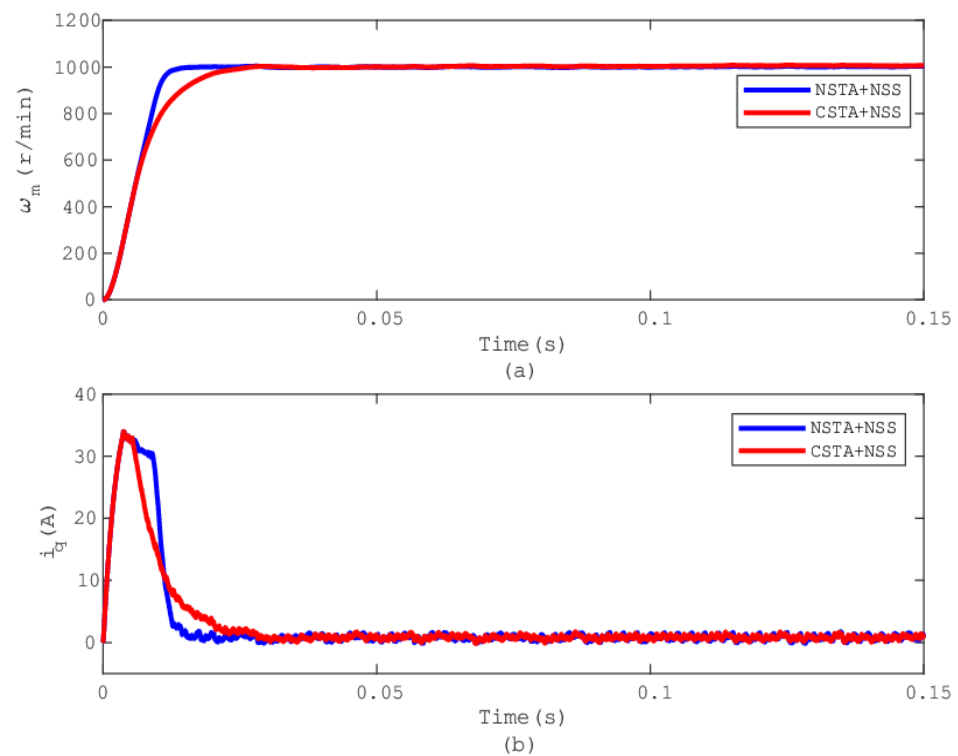**Figure 5.** Comparison of CSTA+NSS and CRL+NSS: (**a**) speed regulation, (**b**) control action.

Figure 6. Comparison of NSTA+NSS and CSTA+NSS: (**a**) speed regulation, (**b**) control action.
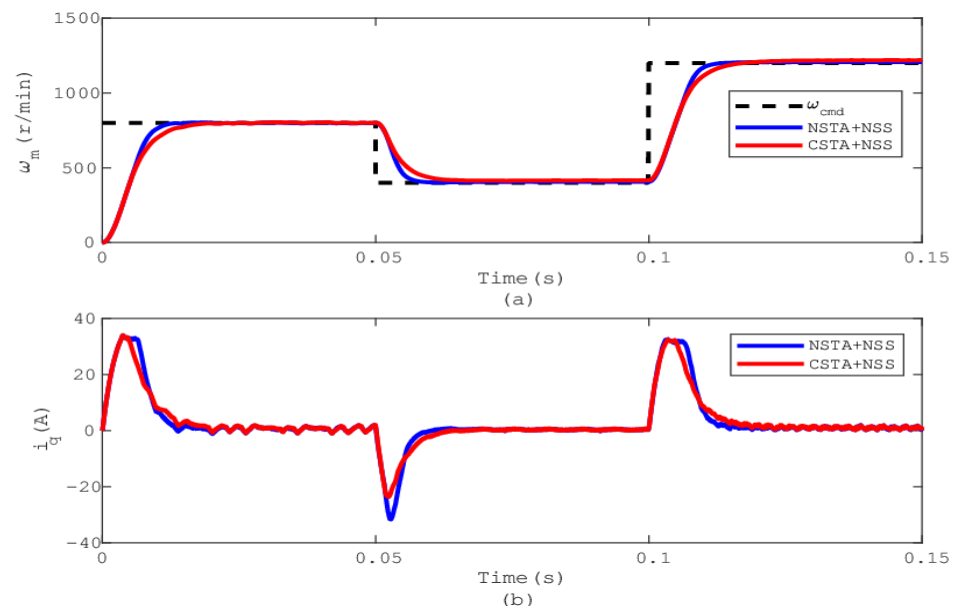
Figure 7. Comparison of NSTA+NSS and CSTA+NSS: (**a**) speed tracking, (**b**) control action.

In case IV, since the ESO can handle external disturbances and improve the control performance of the system [31], we appended the ESO to the NSTA+NSS and compared it with the NSTA+NSS, as shown in Figures 8 and 9, to illustrate the speed regulation, speed tracking, and corresponding current (control action) changes. The results shown in Figure 8a demonstrate that the NSTA+NSS produced overshoot and oscillation after the disturbance (torque as a disturbance in this study) was added. However, overshoot and oscillation could be greatly reduced when the ESO is involved in the NSTA+NSS. Furthermore, the current changes quickly and smoothly due to the ESO, as shown in Figure 8b. Figure 9a demonstrates that the NSTA+NSS with the ESO adapts better than the NSTA+NSS to speed changes when the desired speed drops from 800 rpm to 400 rpm at 0.04 s and increases again from 400 rpm to 1200 rpm at 0.08 s. The effect observed in Figure 8b is confirmed in Figure 9b due to the ESO.
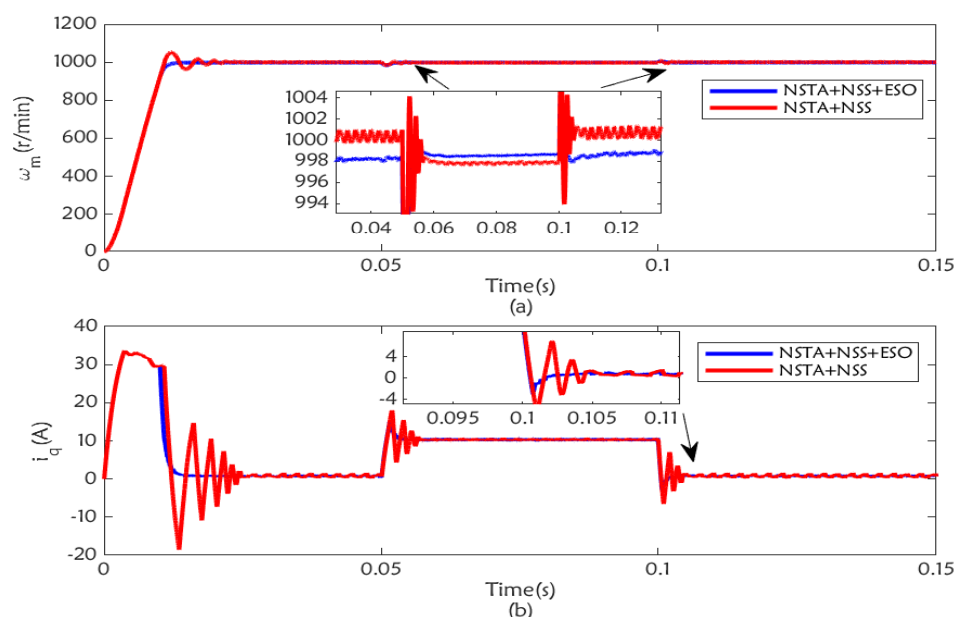

Figure 8. Comparison of NSTA+NSS+ESO and NSTA+NSS: (**a**) speed regulation, (**b**) control action.
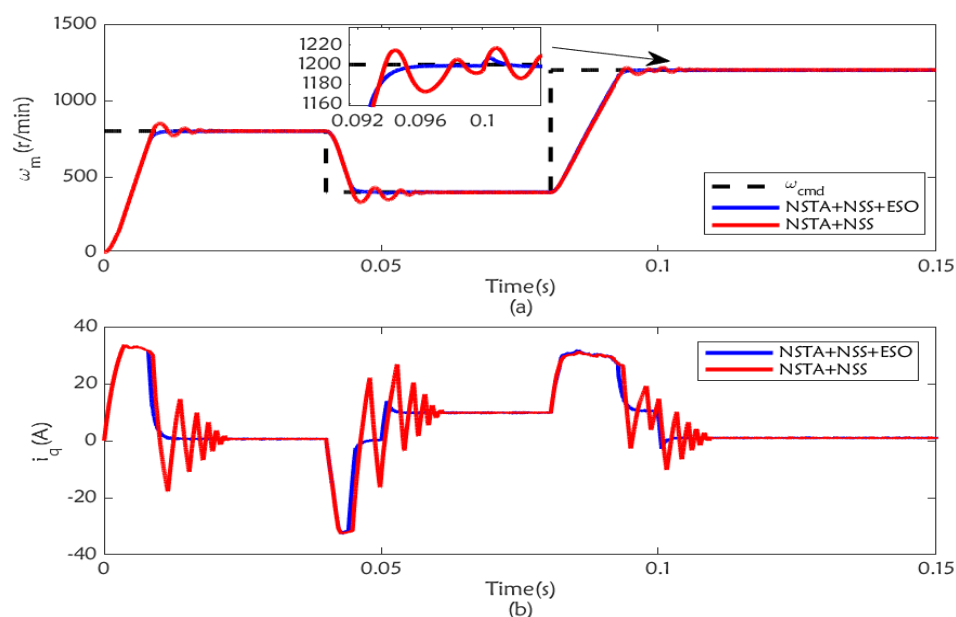
Figure 9. Comparison of NSTA+NSS+ESO and NSTA+NSS: (**a**) speed tracking, (**b**) control action.

6. Conclusions

A strategy combining an NSTSMC and ESO was proposed to improve the anti-disturbance capability of a PMSM system. After combining the NSTSMC and ESO, we performed an overall analysis to ensure the stability of the entire speed loop. In the NSTSMC+ESO method, the adaptive law was used to estimate the model uncertainty perturbation, and the ESO was employed to estimate the external perturbation. NSTSMC+ESO can achieve the desired control of a PMSM system in the presence of parameter variations and external disturbances since the estimated values were designed as feedback terms for the NSTSMC controller. The validity of the proposed method was verified by comparing the numerical simulation results with those obtained using conventional control methods on a case-by-case basis. After the comparison of the simulation results, the efficiency of the settling time of the NSTSMC+ESO (NSTA+NSS+ESO) increased by 75% compared to the NSTSMC (NSTA+NSS) and 91% compared to the CSTA+NSS. The proposed method can be applied to PMSM systems with extreme parameter variations, especially in cases where the load disturbance of the motor drive system should be estimated online.

Author Contributions: All authors contributed to this paper. K.Y. and M.H. conceived the idea, performed the analysis, and designed the simulations; H.A. and Y.C. carried out the numerical simulations; and H.A., Y.C. and K.Y. co-wrote the manuscript. All authors have read and agreed to the published version of the manuscript.

Institutional Review Board Statement: Not applicable.

Informed Consent Statement: Not applicable.

Data Availability Statement: Data sharing not applicable.

Conflicts of Interest: The authors declare no conflict of interest.

References

1. Alsubaie, H.; Yousefpour, A.; Alotaibi, A.; Alotaibi, N.D.; Jahanshahi, H. Stabilization of Nonlinear Vibration of a Fractional-Order Arch MEMS Resonator Using a New Disturbance-Observer-Based Finite-Time Sliding Mode Control. *Mathematics* **2023**, *11*, 978. [CrossRef]
2. Wang, F.; Li, S.; Mei, X.; Xie, W.; Rodríguez, J.; Kennel, R.M. Model-based predictive direct control strategies for electrical drives: An experimental evaluation of PTC and PCC methods. *IEEE Trans. Ind. Inform.* **2015**, *11*, 671–681. [CrossRef]

3. Kang, H.; Kim, C.; Kim, Y. Position control for interior permanent magnet synchronous motors using an adaptive integral binary observer. *J. Electr. Eng. Technol.* **2009**, *4*, 240–248. [CrossRef]

4. Yang, T.; Deng, Y.; Li, H.; Sun, Z.; Cao, H.; Wei, Z. Fast integral terminal sliding mode control with a novel disturbance observer based on iterative learning for speed control of PMSM. *ISA Trans.* **2022**, *134*, 460–471. [CrossRef]

5. Da, Y.; Shi, X.; Krishnamurthy, M. A novel universal sensor concept for survivable PMSM drives. *IEEE Trans. Power Electron.* **2013**, *28*, 5630–5638. [CrossRef]

6. Shen, H.; Li, F.; Xu, S.; Sreeram, V. Slow state variables feedback stabilization for semi-Markov jump systems with singular perturbations. *IEEE Trans. Autom. Control* **2017**, *63*, 2709–2714. [CrossRef]

7. Brasel, M. A gain-scheduled multivariable LQR controller for permanent magnet synchronous motor. In Proceedings of the 2014 19th International Conference on Methods and Models in Automation and Robotics (MMAR), Miedzyzdroje, Poland, 2–5 September 2014; pp. 722–725.

8. Sun, Z.Y.; Shao, Y.; Chen, C.C.; Meng, Q. Global output-feedback stabilization for stochastic nonlinear systems: A double-domination approach. *Int. J. Robust Nonlinear Control* **2018**, *28*, 4635–4646. [CrossRef]

9. Zuo, Y.; Zhu, X.; Quan, L.; Zhang, C.; Du, Y.; Xiang, Z. Active disturbance rejection controller for speed control of electrical drives using phase-locking loop observer. *IEEE Trans. Ind. Electron.* **2018**, *66*, 1748–1759. [CrossRef]

10. Qu, L.; Qiao, W.; Qu, L. An extended-state-observer-based sliding-mode speed control for permanent-magnet synchronous motors. *IEEE J. Emerg. Sel. Top. Power Electron.* **2020**, *9*, 1605–1613. [CrossRef]

11. Yuan, T.; Zhang, Y.; Chang, J.; Wang, D.; Liu, Z. Improved $H\infty$ repetitive controller for current harmonics suppression of PMSM control system. *Energy Rep.* **2022**, *8*, 206–213. [CrossRef]

12. Karboua, D.; Toual, B.; Kouzou, A.; Douara, B.O.; Mebkhouta, T.; Bendenidina, A.N. High-order supper-twisting based terminal sliding mode control applied on three phases permanent synchronous machine. *Period. Polytech. Electr. Eng. Comput. Sci.* **2023**, *67*, 40–50. [CrossRef]

13. Mohd Zaihidee, F.; Mekhilef, S.; Mubin, M. Robust speed control of PMSM using sliding mode control (SMC)—A review. *Energies* **2019**, *12*, 1669. [CrossRef]

14. Huang, Y.J.; Kuo, T.C.; Chang, S.H. Adaptive sliding-mode control for nonlinearsystems with uncertain parameters. *IEEE Trans. Syst. Man Cybern. Part B (Cybernetics)* **2008**, *38*, 534–539. [CrossRef]

15. Li, Y.; Xu, Q. Adaptive sliding mode control with perturbation estimation and PID sliding surface for motion tracking of a piezo-driven micromanipulator. *IEEE Trans. Control Syst. Technol.* **2009**, *18*, 798–810. [CrossRef]

16. El-Sousy, F.F. Robust wavelet-neural-network sliding-mode control system for permanent magnet synchronous motor drive. *IET Electr. Power Appl.* **2011**, *5*, 113–132. [CrossRef]

17. Ma, Y.; Li, D.; Li, Y.; Yang, L. A novel discrete compound integral terminal sliding mode control with disturbance compensation for PMSM speed system. *IEEE/ASME Trans. Mechatron.* **2021**, *27*, 549–560. [CrossRef]

18. Yang, J.; Li, S.; Su, J.; Yu, X. Continuous nonsingular terminal sliding mode control for systems with mismatched disturbances. *Automatica* **2013**, *49*, 2287–2291. [CrossRef]

19. Che, Z.; Yu, H.; Mobayen, S.; Ali, M.; Yang, C.; El-Sousy, F.F. Dual-time-scale sliding mode control for surface-mounted permanent magnet synchronous motors. *Symmetry* **2022**, *14*, 1835. [CrossRef]

20. Kaplan, O.; Bodur, F. Super twisting algorithm based sliding mode controller for buck converter with constant power load. In Proceedings of the 2021 9th International Conference on Smart Grid (icSmartGrid), Setubal, Portugal, 29 June–1 July 2021; pp. 137–142.

21. Wu, J.; Lu, Y. Adaptive backstepping sliding mode control for boost converter with constant power load. *IEEE Access* **2019**, *7*, 50797–50807. [CrossRef]

22. Hollweg, G.V.; de Oliveira Evald, P.J.D.; Tambara, R.V.; Gründling, H.A. A robust adaptive super-twisting sliding mode controller applied on grid-tied power converter with an LCL filter. *Control Eng. Pract.* **2022**, *122*, 105104. [CrossRef]

23. Mokhtar, M.; Marei, M.I.; El-Sattar, A.A. An adaptive droop control scheme for DC microgrids integrating sliding mode voltage and current controlled boost converters. *IEEE Trans. Smart Grid* **2017**, *10*, 1685–1693. [CrossRef]

24. Ding, S.; Mei, K.; Li, S. A new second-order sliding mode and its application to nonlinear constrained systems. *IEEE Trans. Autom. Control* **2018**, *64*, 2545–2552. [CrossRef]

25. Hou, Q.; Ding, S. GPIO based super-twisting sliding mode control for PMSM. *IEEE Trans. Circuits Syst. II Express Briefs* **2020**, *68*, 747–751. [CrossRef]

26. Li, S.; Zhou, M.; Yu, X. Design and implementation of terminal sliding mode control method for PMSM speed regulation system. *IEEE Trans. Ind. Inform.* **2012**, *9*, 1879–1891. [CrossRef]

27. Meng, Q.; Qian, C.; Liu, R. Dual-rate sampled-data stabilization for active suspension system of electric vehicle. *Int. J. Robust Nonlinear Control* **2018**, *28*, 1610–1623. [CrossRef]

28. Ding, S.; Liu, L.; Zheng, W.X. Sliding mode direct yaw-moment control design for in-wheel electric vehicles. *IEEE Trans. Ind. Electron.* **2017**, *64*, 6752–6762. [CrossRef]

29. Ding, S.; Chen, W.H.; Mei, K.; Murray-Smith, D.J. Disturbance observer design for nonlinear systems represented by input–output models. *IEEE Trans. Ind. Electron.* **2019**, *67*, 1222–1232. [CrossRef]

30. Carpiuc, S.C.; Lazar, C. Fast real-time constrained predictive current control in permanent magnet synchronous machine-based automotive traction drives. *IEEE Trans. Transp. Electrif.* **2015**, *1*, 326–335. [CrossRef]

31. Ren, J.; Ye, Y.; Xu, G.; Zhao, Q.; Zhu, M. Uncertainty-and-disturbance-estimator-based current control scheme for PMSM drives with a simple parameter tuning algorithm. *IEEE Trans. Power Electron.* **2016**, *32*, 5712–5722. [CrossRef]

32. Hou, Q.; Ding, S.; Yu, X. Composite super-twisting sliding mode control design for PMSM speed regulation problem based on a novel disturbance observer. *IEEE Trans. Energy Convers.* **2020**, *36*, 2591–2599. [CrossRef]

33. Wu, Y.J.; Li, G.F. Adaptive disturbance compensation finite control set optimal control for PMSM systems based on sliding mode extended state observer. *Mech. Syst. Signal Process.* **2018**, *98*, 402–414. [CrossRef]

34. Zhang, X.; Hou, B.; Mei, Y. Deadbeat predictive current control of permanent-magnet synchronous motors with stator current and disturbance observer. *IEEE Trans. Power Electron.* **2016**, *32*, 3818–3834. [CrossRef]

35. Deng, Y.; Wang, J.; Li, H.; Liu, J.; Tian, D. Adaptive sliding mode current control with sliding mode disturbance observer for PMSM drives. *ISA Trans.* **2019**, *88*, 113–126. [CrossRef]

36. Wang, Y.; Feng, Y.; Yu, X. High-order nonsingular terminal sliding mode control of uncertain multivariable systems. In Proceedings of the IECON 2007-33rd Annual Conference of the IEEE Industrial Electronics Society, Taipei, Taiwan, 5–8 November 2007; pp. 710–714.

37. Zhang, X.; Sun, L.; Zhao, K.; Sun, L. Nonlinear speed control for PMSM system using sliding-mode control and disturbance compensation techniques. *IEEE Trans. Power Electron.* **2012**, *28*, 1358–1365. [CrossRef]

38. Fallaha, C.J.; Saad, M.; Kanaan, H.Y.; Al-Haddad, K. Sliding-mode robot control with exponential reaching law. *IEEE Trans. Ind. Electron.* **2010**, *58*, 600–610. [CrossRef]